

# Using a Three-Phase Deterministic Model for the Columnar-to-Equiaxed Transition

M. WU and A. LUDWIG

In order to overcome the limitations of previous columnar-to-equiaxed (CET) models, which neglect melt convection and the movement of free equiaxed grains, this article presents a three-phase deterministic CET model. With appropriated multiphase volume-averaging approaches, it is possible to account for nucleation and growth of equiaxed grains ahead of a growing columnar front, the influence of melt convection, and grain sedimentation, and the occurrence of a CET in a casting of engineering scale. Special modeling assumptions ensure that both CET mechanisms, namely, “hard” and “soft” blocking, are tackled. It is highly recommended that both mechanisms should be considered, especially in the situation where grain sedimentation and melt convection are present. Although the current model incorporates almost all the physical variables relevant to a CET event, under special condition of a one-dimensional case, the model still reproduces the results of Hunt’s classical CET approach.

## I. INTRODUCTION

SINCE the first deterministic model of J.D. Hunt in 1984,<sup>[1]</sup> the columnar-to-equiaxed transition (CET) has become one of the most important subjects in solidification research. At that time, Hunt considered a simple one-dimensional steady-state mixed columnar-equiaxed solidification with an imposed thermal gradient,  $G$ , and columnar tip velocity,  $V_{\text{tip}}$ . The columnar tip front is assumed to be correlated with a so-called tip undercooling,  $\Delta T_{\text{tip}}$ , which is determined by a deterministic relation to the imposed  $V_{\text{tip}}$ . The equiaxed grains nucleate and grow ahead of the columnar tip front. It is considered that the grain growth and the evolution of the volume fraction of the equiaxed phase,  $f_e$ , are solved analytically. A “hard blocking” mechanism was proposed to determine the CET: the columnar tips will be blocked when the local  $f_e$  is greater than 0.49. According to this model, the CET is predicted to occur when the following condition is met:

$$G < 0.617 \cdot n_{\text{max}}^{1/3} \left( 1 - \left( \frac{\Delta T'_N}{\Delta T_{\text{tip}}} \right)^3 \right) \quad [1]$$

Fully equiaxed solidification is predicted to occur at low-temperature gradients and high growth velocity. A low nucleation undercooling,  $\Delta T'_N$ , a high density of nuclei,  $n_{\text{max}}$ , and a high alloy concentration,  $c_0$ , can favor the CET. These outcomes were later justified experimentally.<sup>[2,3]</sup> Because of its simplicity, this model cannot be applied to real casting processes. Although the model was later extended to solve

an unsteady temperature field and to track the position of the columnar front explicitly by a parabolic velocity-undercooling relation, *etc.*,<sup>[4,5]</sup> and still later improved to include a more precise dendrite growth model and to consider the concentration profile ahead of the columnar tip front,<sup>[6]</sup> it is still far from being able to predict the CET for real casting processes.

Recent advancements of numerical CET models available at the process scale can be classified according to the type of modeling approach:<sup>[7–12]</sup> stochastic or deterministic. According to Reference 7, the stochastic approach, *i.e.*, the cellular automaton model coupled with macroscopic thermal or solute fields, has the advantage of modeling the details of the columnar and equiaxed morphologies, while the deterministic approach embodies the physical mechanisms involved in the solidification process, especially in regard to convection and grain transport. The model described here is confined to the deterministic approach.

A multiphase/multiscale deterministic model was proposed by Beckermann and his co-workers.<sup>[9]</sup> The physical fundamentals applied to handle the nucleation and grain growth of the equiaxed grains ahead of the columnar tip front are similar to the ones used by Hunt,<sup>[1]</sup> *e.g.*, instantaneous nucleation law and the deterministic relation by Lipton, Glicksman, and Kurz (LGK)<sup>[13]</sup> for the dendrite growth velocity in an undercooled melt. During solidification, three phases were distinguished: solid dendrite, interdendritic liquid phase, and extradendritic liquid phase. The macroscopic thermal field is shared by all phases, and the volume averaged species fields for each phase are solved. The merit of resolving the solute field for each phase is to get a more precise constitutional undercooling in front of the columnar front, which is the driving force for both nucleation and grain growth of the equiaxed grains. The same columnar tip hard blocking mechanism as Hunt’s<sup>[1]</sup> is applied to determine the CET. Beckermann’s model was later modified<sup>[10]</sup> by considering the solutal interactions between the columnar front and the growing equiaxed grains. The columnar tips stop growing as the local melt at the columnar tip position is enriched with solute element and the constitutional undercooling vanishes. This is called “soft blocking,” a new columnar tip blocking mechanism. A series of

M. WU, Group Leader of Numerical Modeling and Simulation and Chair of Simulation and Modeling of Metallurgical Processes, and A. LUDWIG, Professor and Director and Chair of Simulation and Modeling of Metallurgical Processes, are with the Christian-Doppler-Laboratory for Multiphase Modeling of Metallurgical Processes, Department of Metallurgy, University of Leoben, A-8700 Leoben, Austria. Contact e-mail: menghuai.wu@mu-leoben.at

This article is based on a presentation made in the symposium entitled “Solidification Modeling and Microstructure Formation: In Honor of Prof. John Hunt,” which occurred March 13–15, 2006, during the TMS Spring Meeting in San Antonio, Texas, under the auspices of the TMS Materials Processing and Manufacturing Division, Solidification Committee.

parameter studies were carried out; the validity of the model was justified by comparison with the model of Hunt. Furthermore, in the case of unidirectional solidification, comparison with experiments<sup>[14]</sup> showed agreement.

The major drawback of previous CET models at the process scale is that they neglect melt convection and movement of free equiaxed grains. Therefore, the authors recently developed a three-phase model, which aims to tackle the mixed columnar-equiaxed solidification including the CET under the influence of the melt convection and grain sedimentation. The details of this model are presented here, with relevant parameter studies, which expand on previously published<sup>[11,15]</sup> descriptions of the three-phase mixed columnar-equiaxed solidification model.

## II. MODEL OF CET

### A. General Model Description and Assumptions

A Eulerian volume-averaging multiphase approach is used. The different phases, as defined subsequently, are treated mathematically as interpenetrating continua. Volume fractions represent the space occupied by each phase and sum to one. Conservation equations for each phase are derived and solved for the relevant physical variables. Model closure is achieved by providing constitutive relations obtained from solidification dynamics and kinetics, empirical information, or the laws of fluid dynamics. (1) Phase definitions: primary liquid (*l*), equiaxed secondary phase (*e*), and columnar secondary phase (*c*). Their volume fractions,  $f_l$ ,  $f_e$ , and  $f_c$ , are obtained by solving the mass-transport equations with consideration of the mass transfer due to solidification/melting. As shown in Figure 1, in the volume element indexed with  $i_c = 0$ , only equiaxed (*e*) and liquid (*l*) phases coexist, i.e.,  $f_c \equiv 0$ . In the element indexed with  $i_c = 1$ , which includes columnar tips, all three phases coexist. In the element indexed with  $i_c = 2$ , which has already been passed by the columnar front, again all three phases are allowed to coexist

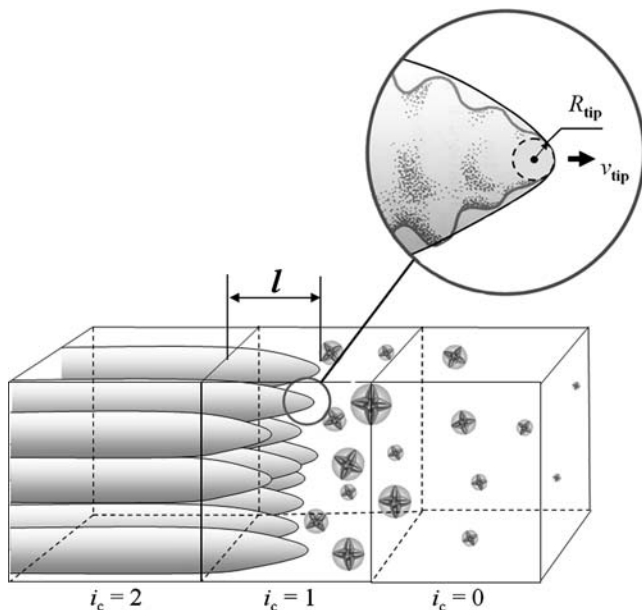


Fig. 1—Schematic diagram of the control volumes in the vicinity of the columnar tip front.

(not necessary). (2) Both primary and equiaxed phases are moving phases, for which the corresponding Navier–Stokes equations are solved for the velocity fields  $\mathbf{u}_l$  and  $\mathbf{u}_e$ . The columnar phase is assumed to solidify from the wall toward the bulk melt and remain stationary; thus, no momentum equation for the columnar phase is considered. (3) Enthalpy equations for all three phases are solved. Due to the fact that thermal diffusion is much higher than solute diffusion, we assume that only one temperature represents each volume element. Therefore, a large volume heat-transfer coefficient between the phases is applied to balance the temperatures of the phases in each element.<sup>[16,17]</sup> (4) Three volume-averaged concentrations,  $c_l$ ,  $c_e$ , and  $c_c$ , are solved. As shown in Figure 2, we assume that the thermodynamic equilibrium condition always applies at the liquid–solid interface. Therefore, an equilibrium concentration of liquid,  $c_l^*$ , is calculated according to the local temperature,  $T$ , based on the phase diagram. The constitutional undercooling ( $c_l^* - c_l$ ) serves as the driving force for solidification. (5) Ideal morphologies for both solid phases are assumed: spheres for equiaxed (globular) grains and cylinders for columnar (cellular) dendrite trunks. As shown in Figures 1 and 2, the grain growth is controlled by diffusion according to the analytically solved concentration profiles around the corresponding crystal (Section B). (6) The columnar grains are assumed to originate from the mold wall. Neither nucleation of columnar grains nor equiaxed-to-columnar transition is taken into account. (7) A continuous three-parameter (Gaussian) heterogeneous nucleation law is applied to model the equiaxed grain nucleation.<sup>[8,11,16,17]</sup> Transport of the grains is also considered. Grain fragments brought into the mold during filling, further fragmentation of dendrites during solidification, and the attachment of equiaxed grains into columnar tips (as a part of the columnar phase) are ignored. (8) The grain size,  $d_e$ , the grain number density,  $n$ , of equiaxed grains, and the diameter,  $d_c$ , of the columnar trunks are explicitly calculated, while a constant value for the primary arm spacing,  $\lambda_1$ , of columnar dendrites is used in this article. (9) Shrinkage porosity

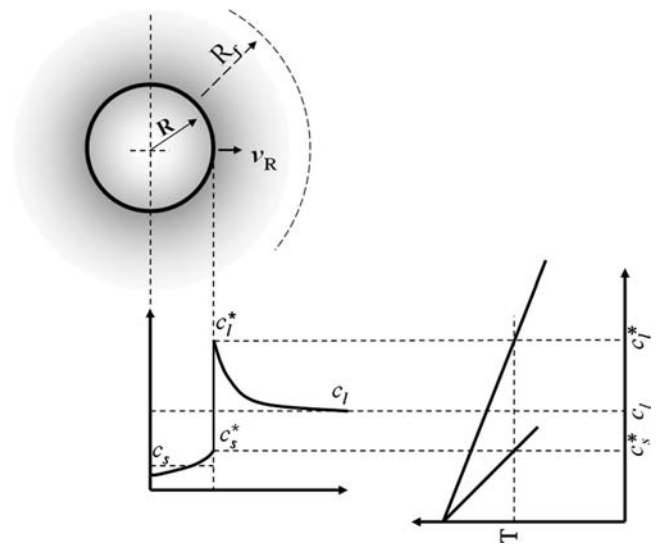


Fig. 2—Schematic principle of diffusion-controlled crystal growth. For equiaxed grains,  $R$  denotes the radius of the grain ( $d_e/2$ ). For the columnar grains,  $R$  denotes half of the diameter of the columnar trunk ( $d_c/2$ ).

is not considered. The Boussinesq approach is employed to model thermosolutal convection, grain sedimentation, and sedimentation-induced melt convection. Feeding flow in the mushy zone can also be modeled when an open calculation domain (e.g., in continuous casting hot melt is conducted through an inlet continuously to feed the shrinkage).<sup>[18]</sup>

### B. Diffusion-Controlled Growth and Volume-Averaged Mass-Transfer Rates

To close the mass-transport equations, one needs to define the volume-averaged net mass-transfer rate,  $M_{le}$  and  $M_{lc}$  ( $\text{kg} \cdot \text{m}^{-3} \cdot \text{s}^{-1}$ ), during solidification. As shown in Figure 2, solidification is governed by species diffusion.

In the case of globular equiaxed solidification, the grain growth velocity,  $v_{R_e}$  ( $\text{m} \cdot \text{s}^{-1}$ ), can be solved analytically via<sup>[19]</sup>

$$v_{R_e} = \frac{dR_e}{dt} = \frac{D_l}{R_e} \cdot \frac{c_l^* - c_l}{c_l^* - c_s^*} = \frac{D_l}{R_e(1-k)} \cdot \left(1 - \frac{c_l}{c_l^*}\right) \quad [2]$$

Here,  $c_l^*$  and  $c_s^*$  ( $=kc_l^*$ ) are the equilibrium liquid and solid concentrations adjacent to the solid/liquid interface, where  $c_l^* = (T - T_f)/m$ . A binary alloy system is considered here. The term  $T_f$  is the melting point of the pure alloy (primary) element,  $m$  the liquidus slope, and  $k$  the partitioning coefficient. The term  $D_l$  is the diffusion coefficient in the liquid, and  $R_e$  ( $=d_e/2$ ) is the radius of the equiaxed grains. If we have solved the grain number density  $n$  ( $\text{m}^{-3}$ ) and the average grain size  $d_e$  ( $m$ ), then the total surface area of the spherical grains per volume can be calculated:  $S_A = n \cdot \pi d_e^2$ . With Eq. [2], we can get the net volume-averaged mass-transfer rate for the globular-equiaxed solidification by taking an Avrami factor ( $f_l$ ) into account for the impingement of the growing grains:

$$M_{le} = v_{R_e} \cdot (n \cdot \pi d_e^2) \cdot \rho_e \cdot f_l \quad [3]$$

As shown in Figure 1, equiaxed grains can exist in all types of volume elements ( $i_c = 0$  to 2). Therefore, Eq. [3] is applicable for all volume elements.

In the case of columnar solidification, two states of the local volume elements must be distinguished (Figure 1): (1) volume elements that have been passed by the columnar tips,  $i_c = 2$ ; and (2) volume elements that contain the columnar tips,  $i_c = 1$ . The columnar tip front is tracked by a method described in Section C. Volume elements indexed with  $i_c = 0$  indicate no columnar dendrite; thus,  $M_{lc} = 0$ .

For the volume elements ( $i_c = 2$ ) that have been passed by the tip fronts, a diffusion-controlled growth model around the columnar trunks is used. Similar to the growth of spherical grains, the growth velocity in the radial direction of such a cylindrical trunk is

$$v_{R_c} = \frac{dR_c}{dt} = \frac{D_l}{R_c} \cdot \frac{c_l^* - c_l}{c_l^* - c_s^*} \ln^{-1} \left( \frac{R_f}{R_c} \right) \quad [4]$$

where  $R_c = d_c/2$  is the average radius of a columnar dendrite trunk, and  $R_f = \lambda_1/\sqrt{\pi}$  is the maximum radius of a columnar dendrite trunk. If the columnar trunks are aligned,

the total surface area of columnar trunks per volume is  $S_A = \pi d_c/\lambda_1^2$ . If the columnar trunks are staggered, the total surface area of columnar trunks per volume is  $S_A = \frac{2}{\sqrt{3}} \cdot \frac{\pi d_c}{\lambda_1^2}$ . Here, we assume that they are in alignment, so we define the net volume-averaged mass-transfer rate for those volume elements as

$$M_{lc} = v_{R_c} \cdot (\pi d_c/\lambda_1^2) \cdot \rho_c \cdot f_l \quad [5]$$

As mentioned previously, both columnar and equiaxed phases are allowed to coexist in these elements ( $i_c = 2$ ). Therefore, both Eqs. [3] and [5] must be applied to determine the net mass-transfer rate from the liquid phase to the equiaxed phase  $M_{le}$  and to the columnar phase  $M_{lc}$ . Both the entrapped equiaxed grains and the columnar trunks grow competitively in these elements.

For the elements containing growing columnar tips ( $i_c = 1$ ), the net mass-transfer rate  $M_{lc}$  is

$$M_{lc} = v_{R_c} \cdot n_c \cdot (\pi d_c \cdot l) \cdot \rho_l \cdot f_l + v_{\text{tip}} \cdot n_c \cdot (\pi R_{\text{tip}}^2) \cdot \rho_l \cdot f_l \quad [6]$$

The first term on the right-hand side of Eq. [6] denotes the net mass-transfer rate due to growth in radial direction of the columnar trunks, and the second term denotes growth of the columnar tips in the columnar axial direction. The actual length,  $l$  (Figure 1), of the columnar dendrites in this volume element is explicitly calculated (Section C). The average number of columnar trucks per volume is  $n_c = 4f_c/(\pi d_c^2 \cdot l)$  for both staggered and aligned columnar trunks. The dendrite tip velocity,  $v_{\text{tip}}$ , and the tip radius,  $R_{\text{tip}}$ , are calculated according to References 13 and 19. Obviously, in this kind of volume element ( $i_c = 1$ ), both columnar and equiaxed phases coexist. Therefore, both Eq. [3] and [6] must be applied to determine  $M_{le}$  and  $M_{lc}$ .

### C. Columnar Tip Front Tracking Algorithm and Prediction of CET

The columnar grains are assumed to originate from the mold wall. The columnar tip front advances with the tip velocity  $v_{\text{tip}}$ . No specific growth-preferred crystalline orientation is imposed. The columnar front is assumed to advance in the preferred direction closest to the temperature gradient due to the fact that the global solidification sequence is governed by the heat extraction of the mold. The position of the columnar tip front is explicitly tracked. The procedure to track the columnar tip front is described subsequently and shown as a schematic diagram in Figure 3. As an example, the calculation domain of Figure 3 is meshed with triangular elements. It is worth mentioning that the following columnar tip front tracking procedure applies to structured and unstructured meshes, and both two-dimensional (2-D) and three-dimensional (3-D) simulations. (1) Each control volume element is indexed with a columnar status,  $i_c$ , which indicates whether the control volume element contains the columnar tip front ( $i_c = 1$ ), or the control volume has been passed by the columnar tips ( $i_c = 2$ ), or the control volume is still in the bulk region where no columnar tip reaches yet ( $i_c = 0$ ). All control

volume elements are initialized with  $i_c = 0$ , except the boundary (wall) elements, which are marked with  $i_c = 1$ . The status marker with  $i_c = 1$  indicates that the columnar grains will start to grow from these boundary elements. (2) A reference length,  $l_{ref}$ , is initially assigned to each control volume. This reference length is used to determine how long it takes for the columnar front to grow out of a volume element. It is defined as an equivalent sphere (or circle in the 2-D case) with a diameter of  $l_{ref}$ . The volume of the sphere must be equal to that of the corresponding control volume element,  $\frac{4\pi}{3} \cdot (l_{ref}/2)^3 = \Delta V$ , in 3-D. One may argue that the chosen definition for  $l_{ref}$  would influence the accuracy of the CET calculation. Therefore, parameter studies are carried out in this article to support the assumed definition of  $l_{ref}$ . (3) The columnar front is assumed to grow in the direction closest to the temperature gradient with a growth velocity,  $v_{tip}$ , determined by the LGK model.<sup>[13,19]</sup> The average length of the columnar grains in the tip volume element ( $i_c = 1$ ) is calculated by the integral  $l = \int_t v_{tip} dt$ ,

starting from the moment when the front enters the control volume element. (4) As soon as  $l$  exceeds  $l_{ref}$ , the columnar tip front is modeled to grow out of the considered volume element. In this case, the neighboring control volume elements, which are still indexed with  $i_c = 0$ , will be reached by the columnar tip front. The status of those neighboring elements is changed to  $i_c = 1$ . The status of the first volume element, which has just been passed by the columnar front, is then set to  $i_c = 2$ . (5) Mass transfer from the liquid to the columnar phase is only taken into consideration for those elements where  $i_c \neq 0$ . Mass transfer from the liquid to the equiaxed phase can occur in all types of volume elements when a certain undercooling for nucleation and growth is achieved. (6) For the mechanical interaction between the two solid phases, a simple approach is used. Both columnar and equiaxed phases are allowed to coexist in the same volume element, even behind the columnar tip elements. When the local volume fraction of the columnar phase,  $f_c$ , is more than a critical value, *e.g.*,  $f_c^{free} = 0.2$ , an infinite drag force coefficient is applied between the two solid phases in the corresponding momentum equations, and thus the equiaxed grains are modeled to be “captured” by the columnar phase. When  $f_c$  is smaller than  $f_c^{free}$ , no drag force is applied; thus, the motion of the equiaxed grains is not affected by the columnar dendrite tips. The validation of the critical value  $f_c^{free} = 0.2$  is also discussed in this article. (7) The columnar tip blocking mechanism described by Hunt<sup>[1]</sup> is implemented to model the CET. In the columnar tip elements, the tip growth velocity,  $v_{tip}$ , is set to zero as soon as the local volume fraction of the equiaxed grains,  $f_e$ , exceeds the critical threshold of  $f_{e,CET} = 0.49$ . The so-called soft blocking mechanism for establishing the CET, proposed by Martorano *et al.*,<sup>[10]</sup> is included, because  $v_{tip}$  vanishes when the local constitutional undercooling disappears.

### III. CET IN UNIDIRECTIONAL SOLIDIFICATION

#### A. Benchmark Definition

A transient unidirectional solidification process is shown in Figure 4. To analyze the phase evolution caused by the

competitive growth of the columnar and equiaxed grains, convection and grain sedimentation are ignored in this benchmark. A simple binary Fe-0.34 wt pct C alloy is considered. The reasons for choosing this alloy are as follows: (1) the mixed columnar-equiaxed solidification with CET event is evidenced in many steel castings; (2) the current model can only handle binary alloys; and (3) the thermophysical and dynamic properties for this alloy are available, as shown in previous publication.<sup>[11]</sup> The process parameters are as follows: initial melt temperature of 1805 K, heat-transfer coefficient between the casting and mold wall of  $200 \text{ W} \cdot \text{m}^{-2} \cdot \text{K}^{-1}$ , and constant wall temperature of 500 K. The nucleation parameters for the equiaxed grains<sup>[8,16,17]</sup> are as follows: the maximum available nucleation sites  $n_{max} = 10^{10} \text{ m}^{-3}$ , the critical nucleation undercooling at which the maximum nucleation rate will be achieved  $\Delta T_N = 3 \text{ K}$ , and the standard deviation of the nucleation  $\Delta T_\sigma = 1 \text{ K}$ . In Section III-D, the process parameters are varied to study their influence on the CET event.

#### B. Phase Evolution and the CET Event

The modeling results are shown in Figures 5 and 6. The volume fractions,  $f_c$  and  $f_e$ , together with the columnar tip

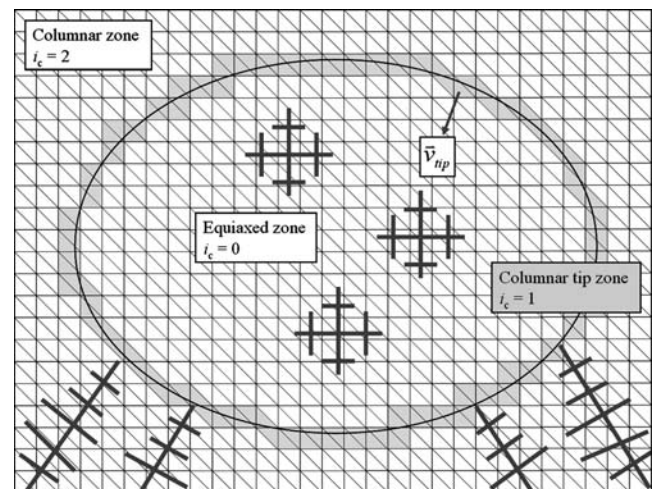


Fig. 3—Schematic diagram of the advance of the columnar tip front, and the algorithm of the columnar front tracking during mixed columnar-equiaxed solidification.

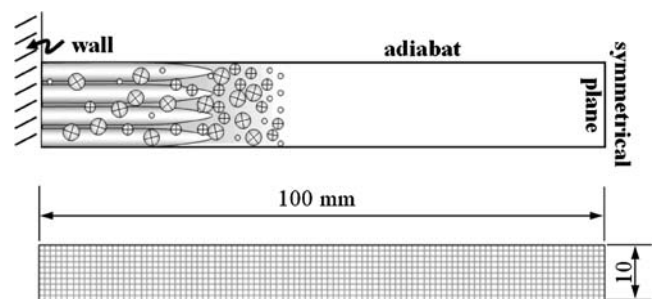
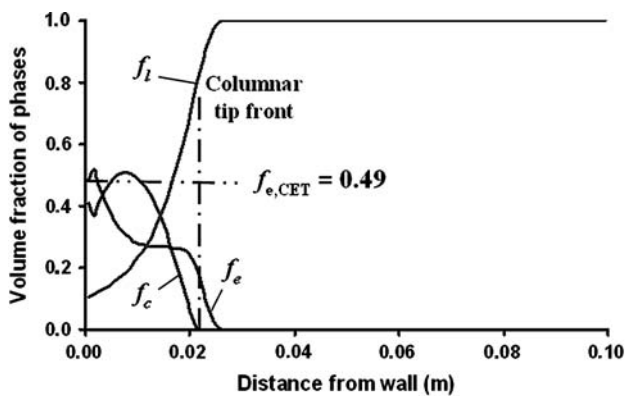


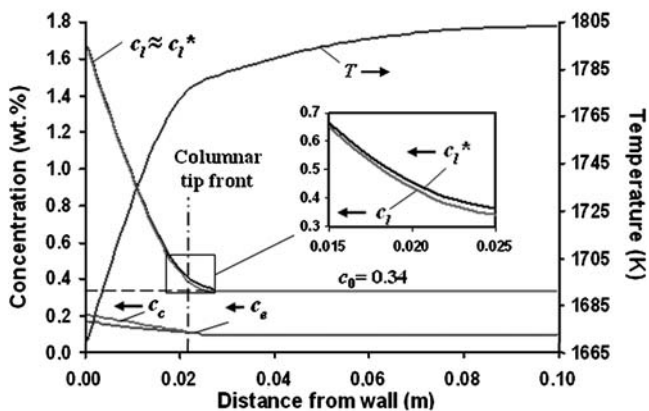
Fig. 4—Configuration of the benchmark for unidirectional solidification. The domain is enmeshed into rectangular volume elements of  $1 \times 1 \text{ mm}$  in size.

position (dashed line with single dots) provide the information about the competitive growth of both phases. A reference line (dashed line with double dots) of  $f_{e,CET} = 0.49$  is given together with the phase fractions to determine the CET event by the mechanism of hard blocking. The volume-averaged liquid concentration,  $c_l$ , together with the liquid equilibrium concentration,  $c_l^*$ , provide information about the solidification driving force, *i.e.*, the constitutional undercooling,  $c_l^* - c_l$ , where  $c_l^* = (T - T_f)/m$ .

The columnar tips are initialized as boundary conditions from the wall boundary elements. Due to undercooling, the columnar phase  $f_c$  evolves immediately in those boundary elements according to Eq. [6]. When the columnar tips grow out of the wall elements, Eq. [5] is used. One would expect that at the very initial stage the evolution of the columnar phase leads the solidification process because the nucleation of the equiaxed grains needs some time to develop. In this benchmark simulation, however, this situation is hardly seen. The nucleation event takes place almost immediately following initialized cooling. A high undercooling is achieved in the vicinity of the wall region. With the nucleation parameters used in this study, a very large number of grains are created very soon. As seen in Figure 5, at  $t = 167$  s, there are even more equiaxed phase  $f_e$  than columnar  $f_c$  near the surface region. In the mixed columnar-equiaxed region, the competitive growth of both phases is actually the result of using Eq. [3] vs Eq. [5].



(a)

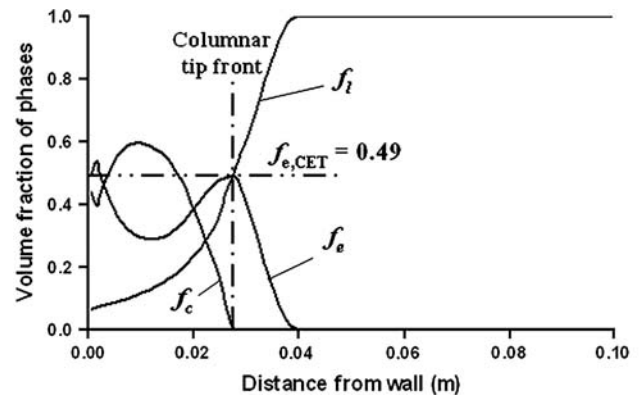


(b)

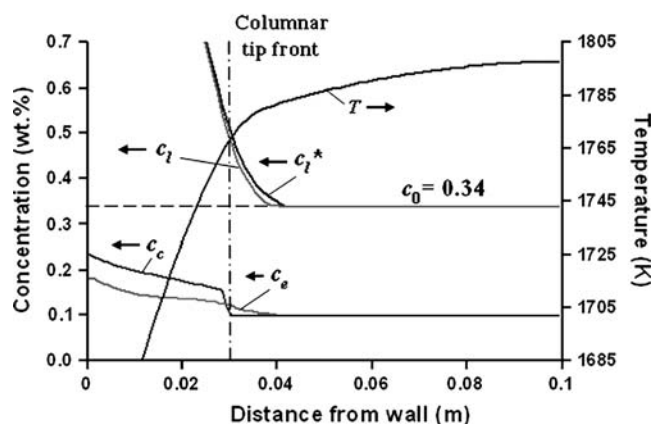
Fig. 5—Phase evolution and corresponding concentration fields at  $t = 167$  s.

It is evidenced that the advancement of the columnar tips is slower than the thermal isotherm. The necessary undercooling for the nucleation of the equiaxed grains can be achieved ahead of the columnar tips. Therefore, there is always equiaxed phase ahead of the columnar tips. At  $t = 167$  s, the phase fraction of the equiaxed grains at the columnar tip position is about 0.2, but it is still below the blocking criterion ( $f_{e,CET} = 0.49$ ). This means that the columnar tips are still free to grow if the constitutional undercooling,  $c_l^* - c_l$ , exists.

Another interesting result obtained is that the columnar tip position is found to be located at a temperature of  $T = 1775.9$  K, which is 6.4 K below the equilibrium liquidus temperature  $T_L^{c_0} = 1782.3$  K ( $T_f + m \cdot c_0$ ) if the initial concentration,  $c_0$ , is referred to. Because the equiaxed solidification is ahead of the columnar tips, the local melt at the columnar tip position is enriched with solute element. The value of  $c_l$  is predicted to be 0.415 wt pct (larger than  $c_0 = 0.34$  wt pct) there. The actual liquidus temperature, considering the enrichment of the solute element, is  $T_L^{c_l} = 1777.8$  K ( $T_f + m \cdot c_l$ ). In other words, the actual undercooling, considering the solute enrichment, is only 1.9 K, corresponding to the constitutional undercooling,  $\Delta c = c_l^* - c_l = 0.0225$  wt pct. This result verifies that the solute enrichment ahead of the columnar tips has an influence on the columnar growth. The influence includes two aspects.



(a)



(b)

Fig. 6—Phase evolution and corresponding concentration fields at  $t = 296$  s. The columnar tip front is blocked by the equiaxed grains at this moment.

The first one is the reduction of the columnar tip velocity,  $v_{\text{tip}}$ , due to the declining  $\Delta c$ . The  $v_{\text{tip}}$  would be overestimated if the solute enrichment caused by the equiaxed solidification ahead of columnar tip front is ignored. The second aspect is the enhancement of the soft blocking mechanism when  $\Delta c$  vanishes due to the solute enrichment.

Using the hard blocking mechanism, the CET event is predicted to occur at  $t = 296$  s (Figure 6). As the columnar tip front advances to the position of 0.028 m from the mold wall, the equiaxed phase reaches the critical blocking limit,  $f_{e,\text{CET}} = 0.49$ . The columnar tip front stops advancing, although constitutional undercooling still exists ( $\Delta c = 0.0173$ ). In this case, the hard blocking mechanism operates before the driving force for columnar tip growth,  $\Delta c$ , vanishes.

Nucleation of equiaxed grains occurs mainly ahead of the columnar tip fronts. From the results of Figures 5 and 6, it is evident that the movement of the columnar tip front is delayed (depressed) in comparison to the starting point for the nucleation and evolution of the equiaxed phase. The reason is, once again, the solute enrichment due to equiaxed solidification ahead of the columnar tip front. With time, the delay between the equiaxed starting point and the columnar tip front tends to become wider and wider, until the CET occurs. The current model assumes a simple spherical morphology for the equiaxed grains. One may argue that the solute rejection by the globular grains can be overestimated in comparison to that by the grains with dendritic morphology. To take the dendritic morphology into account, as was done in References 9 and 10, additional phases for the interdendritic liquid would have to be considered, which is beyond the scope of this article.

After the CET event, the columnar tip front remains stationary, although the solidification process goes on. The equiaxed grains continue to nucleate and grow in the bulk melt. In the mean time, the columnar trunks grow thicker and grow competitively with the coexisting equiaxed grains behind the columnar tip front. The continuously enriched solute element in the interdendritic region,  $c_l$ , may reach the eutectic point,  $c_E$ . Here, the phase transition from the residual melt to the eutectic is simplified. However, the modeling result allows estimation of the volume fraction of the eutectic phase. The model is simplified such that when  $c_l$  reaches the eutectic point ( $c_E$ ), the mass-transfer rates of both  $M_{lc}$  and  $M_{le}$  are set to 0. The volume fraction of the rest of the melt remains unchanged as eutectic. This simplification is reasonable only when the rest of the eutectic phase is minor in comparison with the primary solid phases, because the effect of the latent heat released by the eutectic reaction is ignored.

### C. Hard Blocking and Soft Blocking

In order to understand the mechanism of hard blocking and soft blocking, an additional simulation was carried out with the same configuration as Figure 4 and the same physical and process parameters. The only modification was to “switch off” the function of the hard blocking, letting the columnar tip front continue to advance, even if the equiaxed volume fraction exceeds the  $f_{e,\text{CET}}$  at the columnar tip front, until the columnar tip front stops growing due to the disappearance of the driving force for the columnar tip growth,  $c_l^* - c_l$ .

As shown in Figure 7(a), the columnar tip velocity,  $v_{\text{tip}}$ , decreases with the advance of the columnar tip front. The reason for this is the enrichment of the solute element,  $c_l$ , caused by the equiaxed solidification ahead of the columnar tips. According to the LGT model,<sup>[13,19]</sup> the  $v_{\text{tip}}$  decreases with the decrease of the constitutional undercooling,  $c_l^* - c_l$ . If no hard blocking occurs, the columnar tips can advance to the farthest position, 0.0395 m from the wall, where  $v_{\text{tip}}$  tends to be 0. This end position defines the CET point by the mechanism of soft blocking. In Figure 7(b), the volume fraction distributions of equiaxed phase at four different moments (70, 167, 296, and 1542 seconds) are also shown:  $f_e(\text{I})$  to  $f_e(\text{IV})$ . The columnar tip front reaches position I (0.0115 m from the wall) at  $t = 70$  s, position II (0.0205 m from the wall) at  $t = 167$  s, and position III (0.028 m from the wall) at  $t = 296$  s. The end position is predicted to be 0.0395 m from the wall.

If we compare the two simulations, hard blocking and soft blocking, the first part of the  $v_{\text{tip}}$  curves are identical until the tip front reaches the position III. With the hard blocking, the columnar tip velocity,  $v_{\text{tip}}$ , is set to zero at position III, because  $f_e$  reaches  $f_{e,\text{CET}}$  at this moment (296 seconds). If hard blocking is disabled, the columnar tip velocity,  $v_{\text{tip}}$ , can continue to advance and reach its farthest position, IV, where the constitutional undercooling

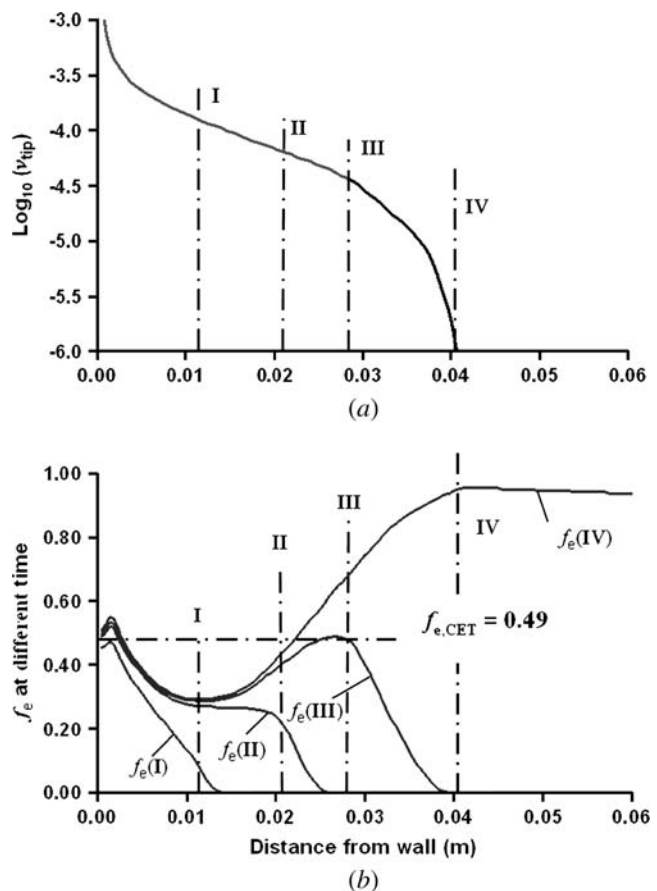


Fig. 7—(a) The columnar tip velocity,  $v_{\text{tip}}$  ( $\text{cm} \cdot \text{s}^{-1}$ ), as function of the columnar tip position; and (b) the volume fraction distributions of the equiaxed phase  $f_e(\text{I})$  to  $f_e(\text{IV})$  at  $t = 70, 167, 296,$  and  $1542$  s. The dashed lines labeled with I to IV indicate the columnar tip positions at  $t = 70, 167,$  and  $296$  s, and the end position, respectively.

vanishes. Figure 8 shows the final phase distributions of the two different columnar tip blocking mechanisms. According to these results, the phase distributions are identical beyond position IV, and they are almost the same behind position III. The difference is found in the region between positions III and IV.

Based on these results, both the hard blocking mechanism and the influence of the solute enrichment ahead of the columnar front must be taken into account to predict the CET correctly. According to Reference 10, the columnar tip velocity,  $v_{tip}$ , can be overestimated if based on the initial concentration  $c_0$  rather than the current  $c_l$ . However, if the model is based only on soft blocking, and if the mechanical impingement of the solidified equiaxed grains is ignored, the model would underestimate the CET event. Especially in the comprehensive situation with grain sedimentation and melt convection, as presented in Section IV, the CET event caused by hard blocking would be more pronounced. The preceding benchmark and the alloy chosen for this study appear to favor hard blocking. It is no wonder that one may find that some other alloys and process conditions would favor soft blocking.

#### D. CET Map

In order to generate the CET map, over 20 different simulations were carried out with varying process parameters (initial temperature 1785 to 1805 K, wall temperature 300 to 500 K, and heat-transfer coefficient 100 to 2000  $W \cdot m^{-2} \cdot K^{-1}$ ). Each simulation was run until a CET occurred. The corresponding columnar tip growth velocity,  $v_{tip}$ , at the exact moment when the CET occurs was taken for  $V$ . As the temperature field varies during the transient solidification process,  $G$  at the columnar tip front was also taken at the exact instant of the CET. In Figure 9, the corresponding CET predictions were gathered. Independent of the chosen process parameters, all the CET points fall at a  $\log V$ - $\log G$  plot into a gray band. This gray band divides the plot into two parts: columnar growth (together with equiaxed grains in the columnar mush) in the lower-right part and equiaxed growth only in the upper-left part. This result agrees well with former studies.<sup>[1,19]</sup> With an increasing maximum number density of nuclei from  $n_{max} = 1 \times 10^{10} m^{-3}$  to  $5 \times 10^{10} m^{-3}$ , our model predicts a shift of the CET band toward the lower-right corner of the plot, again, in agreement with Hunt's model.<sup>[1]</sup> Note that many experimental and analytical studies on CET are based on an "imposed" growth velocity,  $V$ , and an imposed temperature gradient,  $G$ . In our configuration, only the process parameters are imposed, whereas  $V$  and  $G$  are obtained as modeling results. Thus, a transient case is compared to a quasi-steady-state consideration. However, concerning the variation range of the process parameters,  $V$  and  $G$  are found to fall into a limited range, being relatively narrow compared to previous studies.<sup>[1,10,19]</sup>

### IV. CET WITH CONVECTION AND GRAIN MOVEMENT

The solidification of a steel ingot with a relatively small size (diameter: 66 mm, and height: 170 mm) was simulated (Figure 10). The same alloy (Fe-0.34 wt pct C) of the last

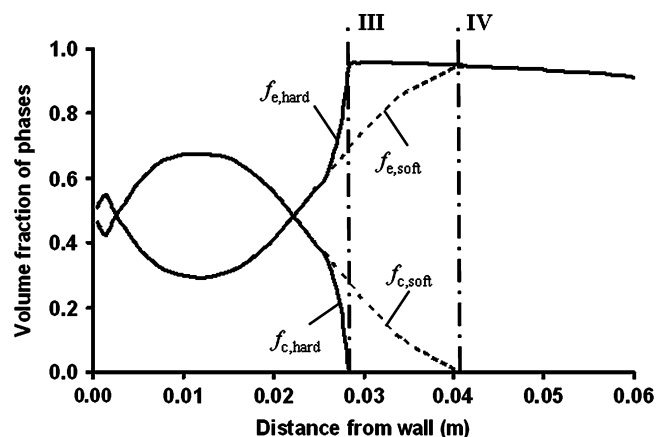


Fig. 8—Final phase distributions predicted by different columnar tip blocking mechanisms: hard blocking and soft blocking. The CET position with hard blocking is marked with dashed line III, and the CET position with soft blocking is marked with line IV.

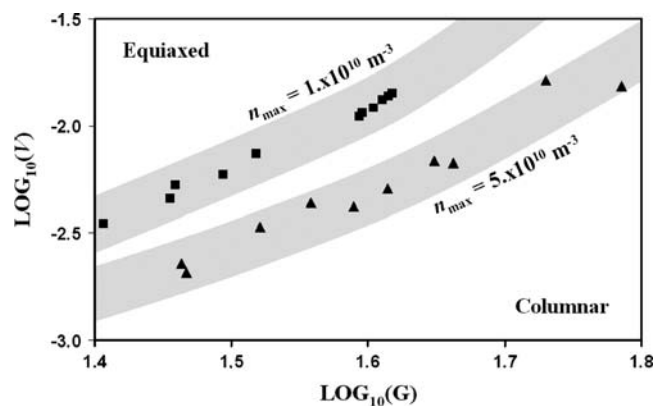


Fig. 9—Predicted CET map for a Fe-0.34 wt pct C alloy. The columnar tip growth velocity,  $v_{tip}$  ( $cm \cdot s^{-1}$ ), at the instant of CET is taken for  $V$ , and the corresponding temperature gradient at the tip position is taken as  $G$  ( $K \cdot cm^{-1}$ ). Heterogeneous nucleation is considered with a three-parameter Gaussian nucleation law, with  $\Delta T_N = 3$  K,  $\Delta T_\sigma = 1$  K, and  $n_{max}$ , as shown in the figure.

benchmark was used. The casting was assumed to be filled instantaneously, so solidification begins with a uniform temperature of 1785 K. The mold and surrounding air are 300 K. Two heat-transfer coefficients were used: 700  $W \cdot m^{-2} \cdot K^{-1}$  between the casting and the mold and 100  $W \cdot m^{-2} \cdot K^{-1}$  between the casting and the air at the top. Nucleation parameters were  $n_{max} = 5 \times 10^9 m^{-3}$ ,  $\Delta T_N = 5$  K, and  $\Delta T_\sigma = 2$  K. Modeling results concerning the evolution of macrostructure and macrosegregation were discussed previously<sup>[11]</sup> by the current authors. Only the importance of the convection and grain sedimentation in the CET is addressed here.

The overall solidification sequence is dominated by heat transfer, but is strongly influenced by melt convection and grain sedimentation. As shown in Figure 10, solidification starts as soon as the surface temperature drops below liquidus. The equiaxed grains start to nucleate near the wall, then sink, and induce melt convection. The melt is dragged downward along the wall by the sinking grains,

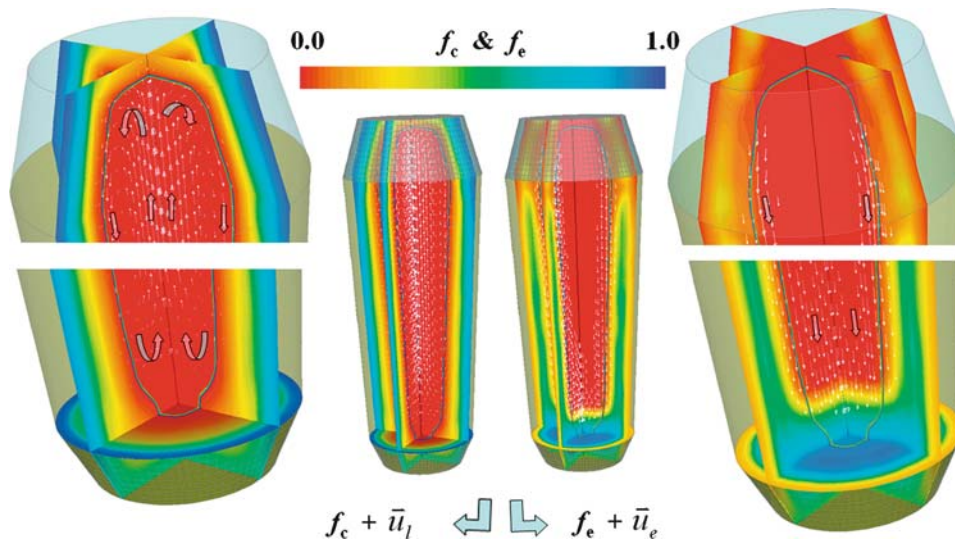


Fig. 10—Modeling result of the solidification sequence at  $t = 20$  s in a steel (Fe-0.34 wt pct C) ingot with a reduced size ( $66 \times 170$  mm o.d.). The volume fraction of the phases  $f_c$  and  $f_e$  are shown in color scale in two vertical and one horizontal section, while the velocity fields  $\mathbf{u}_i$  ( $0$  to  $16 \text{ mm} \cdot \text{s}^{-1}$ ) and  $\mathbf{u}_e$  ( $0$  to  $18 \text{ mm} \cdot \text{s}^{-1}$ ) are shown as vectors. The columnar tip front position is also shown. Left:  $\mathbf{u}_i$  is overlaid with  $f_c$ ; and right:  $\mathbf{u}_e$  is overlaid with  $f_e$ .

which in turn induces a rising melt flow in the middle of the casting, and an axis-symmetrical convection roll is formed. In addition to the grain-sedimentation-induced melt convection, the mechanisms of thermal and solute buoyancy also contribute to the overall melt convection. As solidification progresses, the volume fraction of the columnar phase,  $f_c$ , in the mold wall region increases. In the meantime, the equiaxed grains continue to nucleate in the vicinity of the columnar tip front, sink, and grow. The sedimentation of the equiaxed grains influences the phase distribution. The sinking grains settle and pile up in the lower region of the ingot. This pileup of the equiaxed grains will block the columnar tip front in the lower region of the ingot, causing an enclosed cone shape CET zone. If not enough equiaxed phase exists ahead of the columnar front to block its way, the columnar tip front will meet in the casting center and disappear. This does happen in the upper part of the ingot. Therefore, the final solidification result shows only an enclosed cone shape CET zone in the lower bottom region. The simulated solidification result with the effect of melt convection and grain sedimentation mentioned previously has been speculated for long time based on experimental findings and casting practices.<sup>[20]</sup>

The present model also demonstrated that no CET would occur in this casting when the effects of the melt convection and the grain sedimentation were ignored.<sup>[11]</sup> It is worth mentioning that melt convection and grain sedimentation play the most important role in the macrosegregation formation, a common problem in steel ingots.<sup>[11,21]</sup>

## V. DISCUSSION

The CET is an extremely sensitive event. To predict it, one needs a reliable model, on the one hand, and precise parameters, on the other hand. Influencing factors may arise from different aspects: (1) the alloy, and its thermophysical and thermodynamic properties; (2) process parameters such as initial and boundary conditions; (3) nucleation param-

eters or alternative equiaxed grains generation mechanisms; (4) numerical methods, mesh size, time step, and convergent criteria; (5) model assumptions, *e.g.*, the crystal morphology and the crystal growth kinetics; and (6) parameters used for the columnar front tracking and the CET.

The influence of the alloy concentration on the CET (point 1) has been partially shown by the first CET model of Hunt.<sup>[1]</sup> The influences of points 2 and 3 have been demonstrated in Section III-D (Figure 9). The CET map shows the direct correlation of the CET event to the process conditions and nucleation parameters. Concerning point 4, great care must be taken, especially when multiphase flow phenomenon is involved. A very recent study by Guo and Beckermann<sup>[22]</sup> claimed that the complete grid-independent result seems too difficult to achieve, given present-day computing resources. Concerning the model assumptions (point 5), discussions were made in Reference 11. One limitation of the current model worth mentioning is the dendritic morphology of the growing crystals, for which further development is required.

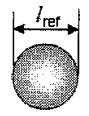
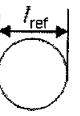
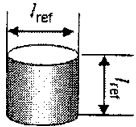
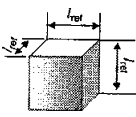
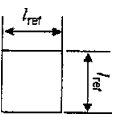
Section A provides more details pertaining to point 6, because the columnar tip tracking algorithm and the model for the interaction between columnar and equiaxed phases use additional parameters such as  $l_{\text{ref}}$  and  $f_c^{\text{free}}$ , for which the uncertainty must be cleared up. The justification of the hard blocking criterion,  $f_{e,\text{CET}} (= 0.49)$ , was done by Hunt.<sup>[1]</sup>

### A. Reference Length $l_{\text{ref}}$

The simulations mentioned previously are based on  $l_{\text{ref}}$ , defined by taking the volume element as an equivalent sphere in 3-D cases, or as an equivalent circle in 2-D and axis symmetrical cases. Some other possibilities are listed in Table I. One speculates about the consequence of choosing different definitions of  $l_{\text{ref}}$ . The ideal situation is that the final modeling result should not be sensitive to the definition of  $l_{\text{ref}}$ .

Two axis symmetrical simulations of the ingot were performed. The first one used the definition  $l_{\text{ref}} = (4 \cdot \Delta V / \pi)^{1/2}$

**Table I. Different Definitions of the Reference Length for a CET**

3-D Volume Element	2-D and Axis Symmetrical Volume Element
	
 $l_{\text{ref}} = (6 \cdot \Delta V / \pi)^{1/3}$	 $l_{\text{ref}} = (4 \cdot \Delta V / \pi)^{1/2}$
 $l_{\text{ref}} = (4 \cdot \Delta V / \pi)^{1/3}$	—
 $l_{\text{ref}} = \Delta V^{1/3}$	 $l_{\text{ref}} = \Delta V^{1/2}$

by taking the volume element as an equivalent circle, while the second used  $l_{\text{ref}} = \Delta V^{1/2}$  by taking the volume element as an equivalent square. It is surprising to find that, although the reference length  $l_{\text{ref}}$  of the second definition is smaller than that of the first definition by a factor of 0.886, the difference between the two modeling results (Figure 11) is minimal. The model with the second  $l_{\text{ref}}$  definition predicted the CET enclosed equiaxed zone to be slightly smaller than the model with the first  $l_{\text{ref}}$  definition.

The reason is as follows. As described in Section II-C and Figure 3, the columnar tips are modeled to move from one volume element to the neighboring elements when the actual columnar length,  $l$ , in the considered volume element grows longer than  $l_{\text{ref}}$ . The smaller the value of  $l_{\text{ref}}$  is, the faster the columnar tips will grow into the neighboring elements. The columnar tip front advances faster with the second, smaller value of  $l_{\text{ref}}$ ; hence, the final CET enclosed equiaxed zone is smaller (Figure 11) than with the first  $l_{\text{ref}}$  definition. However, the columnar tip with the second  $l_{\text{ref}}$  definition does not advance as fast as speculated. The dominant factor for the columnar front is the columnar tip velocity,  $v_{\text{tip}}$ , which is governed by global heat transfer and solute transport. The error caused by the definition of the  $l_{\text{ref}}$  (under- or overestimation) will be leveled out by the global heat and solute balance.

We propose the first definition by taking the volume element as an equivalent circle (2-D). The merit of this definition is to eliminate the factor of topological orientation of the mesh. It does not matter if the columnar grains grow parallel to the direction of a side or to the diagonal of the enmeshed volume element.

To aid the reader in understanding the minor difference of the results shown in Figure 11, two additional modeling

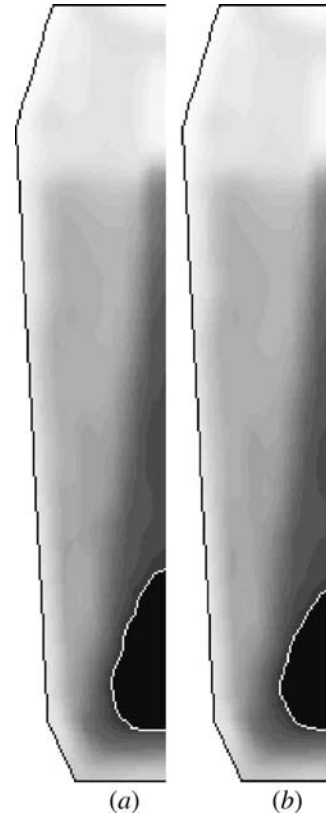


Fig. 11—Predicted CET with different definitions of  $l_{\text{ref}}$ : (a) taking the volume element as an equivalent circle and (b) taking the volume element as an equivalent square. The term  $f_c$  is shown in gray scale with dark for 1 and bright for 0.

examples are worth mentioning. One is the comparison study made by considering or ignoring convection and grain sedimentation.<sup>[11]</sup> With convection and sedimentation included, the final CET result is predicted, as shown in Figure 11(a), while without convection and sedimentation, CET is not predicted at all. Another example shows, by varying the nucleation parameter, that a CET does not occur in this ingot if  $n_{\text{max}}$  is reduced to  $2 \times 10^8$  from  $5 \times 10^9 \text{ m}^{-3}$ .

#### B. Columnar-Equiaxed Interaction and $f_c^{\text{free}}$

No suitable physical model was found to describe the hydrodynamic/mechanical interaction between two solid phases in the mixed columnar-equiaxed region. What one is sure of are the following two extreme cases. When  $f_c$  is sufficiently high, the entrapped equiaxed phase is definitively captured and it is not movable. In the opposite situation, when  $f_c$  is too low, the equiaxed grains are free to move. There might be a range of  $f_c$  in which complicated columnar-equiaxed interactions could occur, depending on the morphological parameters of the phases. The determination of these interactions requires further surveys and studies. Therefore, we only consider the two extreme cases here, and they are separated by a critical value  $f_c^{\text{free}}$ . When

$f_c$  is smaller than  $f_c^{\text{free}}$ , the entrapped equiaxed grains are modeled as freely movable; otherwise, they are captured.

Parameter studies by varying  $f_c^{\text{free}}$  from 0 to 0.4 are carried out, as shown in Figure 12. It is clearly indicated that the modeling result is not significantly sensitive to the chosen value of  $f_c^{\text{free}}$  if it is above 0.2. If  $f_c^{\text{free}}$  falls below 0.2, however, the modeling results are quite different. Therefore, there are still open questions that need further theoretical and experimental study. Can the columnar-equiaxed interaction simply be modeled as done here, with two extreme cases separated by  $f_c^{\text{free}}$ ? If not, an alternative columnar-equiaxed interaction model is required. If yes, the next question is whether  $f_c^{\text{free}}$  falls in the range above or below 0.2. If it is smaller than 0.2, care must be taken in the choice of  $f_c^{\text{free}}$ , and further study is necessary. If it falls in the range above 0.2, the current simple model is accurate. The maximal error caused by an improper value for  $f_c^{\text{free}}$  is seen in Figures 12(c) and (e).

## VI. CONCLUSIONS

A new three-phase mixed columnar-equiaxed solidification model was developed to consider the melt convection and grain sedimentation in the CET. Assumptions are made that the equiaxed grains and the columnar dendrites belong to separated phases with different hydrodynamic behaviors, and their morphologies are simplified as spheres and cylinders, respectively.

1. A 3-D binary Fe-0.34 wt pct C ingot was simulated to demonstrate the potentials of the model. It is able to simulate the mixed columnar-equiaxed solidification including the advance of the columnar front, the evolution of the equiaxed phase ahead of the columnar front, the sedimentation of equiaxed grains, the melt convection, and the occurrence of the CET under the influence of convection and grain sedimentation. The simulation

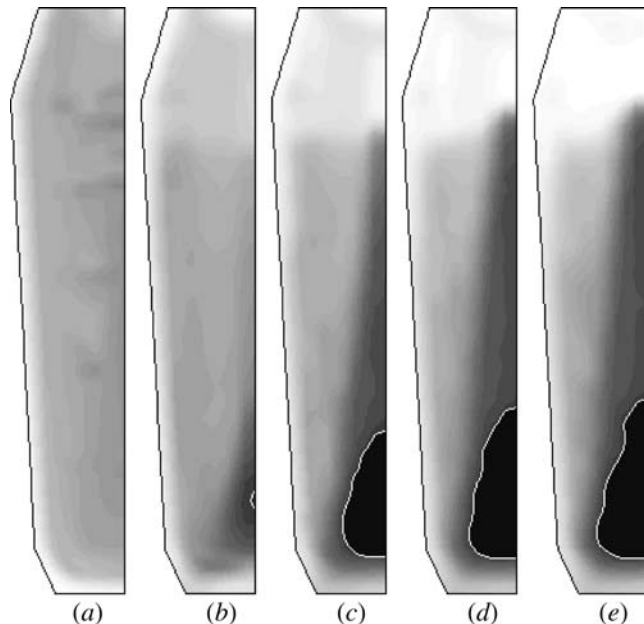


Fig. 12—Predicted CET by varying  $f_c^{\text{free}}$  from 0 to 0.4. The term  $f_c$  is shown in gray scale with dark for 1 and bright for 0.

result qualitatively reproduced the typical experimentally observed solidification phenomena, as reported in the literature.<sup>[20]</sup>

- To understand the phase evolution during mixed columnar-equiaxed solidification, a unidirectional solidification benchmark was simulated. The solute enrichment in the melt ahead of the columnar tip front, due to the species rejection by the solidifying globular equiaxed grains, has significantly reduced the constitutional undercooling at the columnar tips. The advancing velocity of the columnar tip front is declined (depressed) by solute enrichment, due to the solidifying equiaxed grains.
- Two columnar tip blocking mechanisms, *i.e.*, “hard blocking” and “soft blocking,” are compared. The modeling results show that the CET event would be underestimated if only soft blocking is considered. It is highly recommended that both mechanisms should be considered, especially in the situation where grain sedimentation and melt flow are present.
- Parameter studies were made to verify the presented CET model. Uncertainty concerning the model for the hydrodynamic (mechanical) interaction between equiaxed and columnar grains in the columnar tip region is also discussed.

Finally, it must be stated that further refinements to the current model are necessary in both physical modeling and numerical aspects.<sup>[11]</sup>

## NOMENCLATURE

$c_b, c_e, c_c$	species concentration (wt pct)
$c_E$	eutectic concentration of an alloy (wt pct)
$c_l^*, c_s^*$	wt pct equilibrium concentration at liquid-solid interface
$\Delta c = c_l^* - c_c$	wt pct constitutional undercooling
$D_l$	diffusion coefficient ( $\text{m}^2 \cdot \text{s}^{-1}$ )
$d_e$	equiaxed grain diameter (m)
$d_c$	columnar trunk diameter (m)
$f_b, f_e, f_c$	volume fraction of different phases (1)
$f_c^{\text{free}}$	criterion for free moving equiaxed phase in columnar zone (1)
$f_{c, \text{CET}}$	hard blocking criterion (1)
$G$	temperature gradient ahead of columnar tip front ( $\text{K} \cdot \text{m}^{-1}$ )
$i_c$	volume element index for columnar status (1)
$k$	solute partitioning coefficient at the $l/s$ interface (1)
$l$	actual columnar length in tip cell (m)
$l_{\text{ref}}$	reference length of control volume (m)
$M_{le} (= -M_{el})$	liquid-equiaxed net mass transfer rate ( $\text{kg} \cdot \text{m}^{-3} \cdot \text{s}^{-1}$ )
$M_{lc} (= -M_{cl})$	liquid-columnar net mass transfer rate ( $\text{kg} \cdot \text{m}^{-3} \cdot \text{s}^{-1}$ )
$m$	slope of liquidus in phase diagram (K)
$n$	equiaxed grain number density ( $\text{m}^{-3}$ )
$n_c$	columnar trunk number density ( $\text{m}^{-3}$ )
$n_{\text{max}}$	maximum equiaxed grain density ( $\text{m}^{-3}$ )
$R_{\text{tip}}$	columnar tip radius (m)
$R (R_e, R_c)$	grain radius (equiaxed, columnar) (m)
$R_f$	maximum radius of the columnar trunk (m)
$S_A$	surface area of columnar/equiaxed structures per volume ( $\text{m}^{-1}$ )

$T$	temperature (K)
$T_f$	melting point of pure metal (Fe) (K)
$\Delta T$	undercooling (K)
$\Delta T_N$	undercooling for maximum grain production rate (K)
$\Delta T'_N$	undercooling needed in a simultaneous nucleation law (K)
$\Delta T_{\text{tip}}$	undercooling at the columnar dendrite tip (K)
$\Delta T_\sigma$	Gaussian distribution width of nucleation law (K)
$t$	time (s)
$\Delta t$	time-step (s)
$\mathbf{u}_l, \mathbf{u}_e$	velocity vector ( $\text{m}\cdot\text{s}^{-1}$ )
$V$	advancing velocity of columnar tip front ( $\text{m}\cdot\text{s}^{-1}$ )
$v_R (v_{R_c} v_{R_c})$	grain growth velocity in radial direction ( $\text{m}\cdot\text{s}^{-1}$ )
$v_{\text{tip}}$	grain growth velocity in tip direction ( $\text{m}\cdot\text{s}^{-1}$ )
$\Delta V$	volume of the control volume element ( $\text{m}^3$ )
$\lambda_1$	columnar grain space (m)
$\rho$	density ( $\text{kg}\cdot\text{m}^{-3}$ )

### Subscripts

$l, e, c$  liquid, equiaxed, and columnar phases

### REFERENCES

1. J.D. Hunt: *Mater. Sci. Eng.*, 1984, vol. 65, pp. 75-83.
2. R.B. Mahapatra and F. Weinberg: *Metall. Mater. Trans. B*, 1987, vol. 18B, pp. 425-32.
3. I. Ziv and F. Weinberg: *Metall. Mater. Trans. B*, 1989, vol. 20B, pp. 731-34.
4. S.C. Flood and J.D. Hunt: *J. Cryst. Growth*, 1987, vol. 82, pp. 543-51.
5. S.C. Flood and J.D. Hunt: *J. Cryst. Growth*, 1987, vol. 82, pp. 552-60.
6. M. Gäumann, R. Trivedi, and W. Kurz: *Mater. Sci. Eng., A*, 1997, vols. 226-228, pp. 763-69.
7. C.-A. Gandin, T. Jalanti, and M. Rappaz: *Proc. McWASP VIII*, B.G. Thomas and C. Beckermann, eds., TMS, Warrendale, PA, 1998, pp. 363-74.
8. M. Rappaz: *Int. Mater. Rev.*, 1989, vol. 34, pp. 93-123.
9. C.Y. Wang and C. Beckermann: *Metall. Mater. Trans. A*, 1994, vol. 25A, pp. 1081-93.
10. M.A. Martorano, C. Beckermann, and C.-A. Gandin: *Metall. Mater. Trans. A*, 2003, vol. 34A, pp. 1657-74.
11. M. Wu and A. Ludwig: *Metall. Mater. Trans. A*, 2006, vol. 37A, pp. 1613-31.
12. H.B. Dong, X.L. Yang, P.D. Lee, and W. Wang: *J. Mater. Sci.*, 2004, vol. 39, pp. 7207-12.
13. J. Lipton, M.E. Glicksman, and W. Kurz: *Mater. Sci. Eng.*, 1984, vol. 65, pp. 57-63.
14. Ch.-A. Gandin: *Iron Steel Inst. Jpn.*, 2000, vol. 40, pp. 971-79.
15. A. Ludwig and M. Wu: *Mater. Sci. Eng., A*, 2005, vol. 413-414, pp. 109-14.
16. A. Ludwig and M. Wu: *Metall. Mater. Trans. A*, 2002, vol. 33A, pp. 3673-83.
17. M. Wu, A. Ludwig, A. Bührig-Polaczek, M. Fehlbier, and P.R. Sahn: *Int. J. Heat Mass Transfer*, 2003, vol. 46, pp. 2819-32.
18. A. Ludwig, M. Gruber-Pretzler, F. Mayer, A. Ishmurzin, and M. Wu: *Mater. Sci. Eng., A*, 2005, vols. 413-414, pp. 485-89.
19. W. Kurz and D.J. Fisher: *Fundamentals of Solidification*, Trans Tech Publications, Aedemansdorf, Switzerland, 1989, pp. 65-89.
20. J. Campbell: *Castings*, Butterworth Heinemann Ltd., Oxford, United Kingdom, 1991, pp. 151-58.
21. M. Wu, A. Ludwig, M. Pelzer, and U. Postl: *Adv. Eng. Mater.*, 2005, vol. 7, pp. 846-51.
22. J. Guo and C. Beckermann: *Num. Heat Transfer, Part A*, 2003, vol. 44, pp. 559-67.